A Hybrid Testing Framework for Wind Turbine Mechanical Components

F. Nordtorp[1*], E. E. Baş[2], C. Gomes[3] and G. Abbiati[1]

[1]Department of Civil and Architectural Engineering, Aarhus University, Denmark
[2]R&D Test Systems A/S, Hinnerup, Denmark
[3]Department of Electrical and Computer Engineering, Aarhus University, Denmark

[*]E-mail: fnk@cae.au.dk

Abstract. As wind turbines continue to increase in size, hybrid testing is emerging as a key-enabling solution for experimental assessment of their large mechanical components. Hybrid testing is conducted using a hybrid model which combines physically tested and numerically simulated components. In this work, the Kane method is proposed to formulate the equation of motion for the hybrid model of a wind turbine rotor system where one single blade is physically tested. The Kane method allows for formulating the equation of motion of multi-body-dynamic models efficiently and, therefore, it is widely used in state-of-art simulation software. The hybrid model of the rotor is successfully implemented on a single-degree-of-freedom test bench with a cantilever steel beam serving as the physical substructure. The performance of the implemented hybrid model is assessed through a comparison with a pure numerical simulation of the same system. The main finding of the study emphasizes the efficiency of incorporating physically measured restoring force as model parameters while formulating the equation of motion of a hybrid model.

1. Introduction

1.1. Background and motivation

Wind turbines (WT) are complex engineering systems designed to extract energy from the wind and convert it into electrical energy for the power grid. To reduce the *Levelized Cost of Energy*, WT technology is scaling up rapidly, with larger and more efficient components being developed. Testing of WT is crucial to ensure their optimal performance, efficiency, and reliability. Hansen summarizes in [1] the recommended practice to estimate the fatigue damage, which includes monitoring bending moments on blades and tower, yaw and tilt moments on the rotor, axial thrust, torque on the main shaft, and torsional moment on the tower. WT manufacturers face major demands as the cost and duration of testing are increasing in parallel with the upscaling of test benches. Experimental methods that allow for testing large components under realistic critical loading scenarios are needed.

Hybrid testing (HT), also referred to as hardware-in-the-loop simulation (HiL), is an experimental method that allows testing a physical substructure (PS) of an engineering system, while simulating its interaction with the rest of the system in a numerical substructure (NS). Using simulations and controllers realistic critical loading scenarios can be achieved. This method is becoming an increasingly attractive testing technique for cost-efficiently investigating the dynamical response of complex large-scale engineering systems. The concept of HT was

originally introduced in the late 1960s in Japan [2, 3], and has since been applied for mainly the purpose of seismic testing of civil engineering structures. The interested reader can refer to Nakashima et al. [**?**] for a state-of-the-art review, the book of Pan [4] for an overview of the methodology, and the survey in [5].

In the state of the art of HT applied to WT testing, Bosse et al. [6] propose a design for a 4 MW wind turbine generator test system, capable of testing whole nacelles, while simulating the rotor system as a NS. Cheon et al. [7] propose applying the methodology for performance tests of pitch control systems. For HT of structural components, pseudo-dynamic regimes are often sufficient when the PS has a rate-independent restoring force. However, recent improvements in actuation performance have facilitated real-time HT of floating WT with realistic loading conditions. For instance, Sauder et al. [8] propose applying physical hydrodynamic loading on a physical floater in an ocean basin, while simulating the aerodynamic loading and rotor system. Additionally, Belloli et al. [9] propose applying physical aerodynamic loading on a rotor system in a wind tunnel, while simulating the hydrodynamic loads on the floater.

The multi-body-dynamic (MBD) model for simulating the mechanical response of a WT in a HT is typically formulated using Lagrangian, Hamiltonian, or Newton-Euler methods. A prominent technique for solving MBD problems was proposed by Kane et al. [10] in 1965. The Kane method is shown in [11] to outperform other approaches, demonstrating superior efficiency in deriving equations of motion and simplicity in the final equations. The method has become the backbone in reference WT simulation codes like OpenFAST [12] and HAWC2 [13], just to name a few. However, a comprehensive description of how to implement a hybrid MBD model for a WT using the Kane method is currently unavailable to the best of the author's knowledge.

1.2. Scope

This work aims to provide a practical example of applying the Kane method to implement HT for mechanical components of WTs. Specifically, a hybrid MBD model of a simplified 2D WT rotor is presented, wherein one of the three blades is replaced by a physical experiment.

The article is organized as follows: Section 1 introduces the problem and specifies the scope. Section 2 formulates a MBD hybrid model of a WT rotor using the Kane method, section 3 demonstrates an implementation of the hybrid model, and section 4 presents the results from the hybrid test and compares it to a purely numerical simulation of an equivalent system. Finally, section 5 concludes the work.

2. Formulation of MBD hybrid model

A MBD hybrid model is formulated based on the Kane method, for a simplified structural WT rotor system inspired by Hansen [1], as presented in Figure 1. The system consists of a 4-degree-of-freedom (dof) 2D rotor with 3 blades connected to a generator. Each blade is represented by a prematurely linearized cantilever beam, whereas axial deformation is neglected. As a simplification, the mass of each blade is lumped on its tip. The generator is represented by a linear dash-pot. The configuration of the model is thus completely characterized by four generalized coordinates $q_1 - q_4$. The bending deformation for each blade is described by q_1, q_2, and q_3, while q_4 describes the rotational deformation of the hub. The remaining parameters of the models are defined in Table 1.

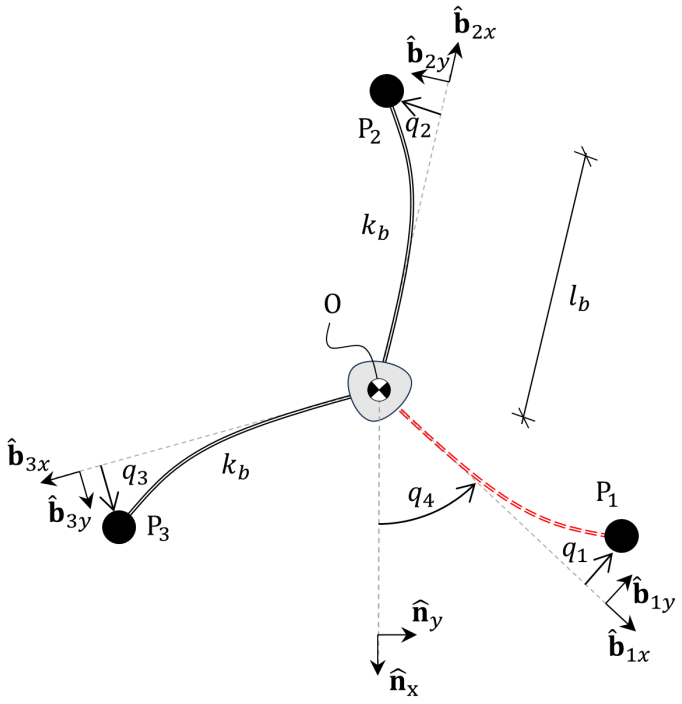

Figure 1: Simplified structural wind turbine rotor system in 2D, inspired by Hansen [1]. The red dashed line represents the physical substructure in the hybrid model. $\hat{\mathbf{n}}_z$ and $\hat{\mathbf{b}}_{iz}$ point outward from the figure.

Table 1: Model parameters for the simplified wind turbine rotor system.

Description	Symbol	Value	Unit
Blade length	l_b	0.5	m
Blade mass	m_b	1.96	kg
Blade mass proportional damping	ζ_b	1	$1/s$
Blade stiffness	k_b	7.2×10^3	N/m
Wind load	f_w	100	N
Geartrain mass of inertia	I_g	0.1	kgm^2
Geartrain damping	d_g	100	Nms
Gravity	g	9.82	m/s^2
Ramping time instance	t_0	0.5	s

Following the procedure for the Kane method from the books of Banerjee [14] and Roithmayr et al. [15], a hybrid model is formulated. To clarify the formulation, instead of presenting the Kane method generically, this section illustrates, in a step-wise fashion, how it is applied to assemble a hybrid model for the outlined simplified WT rotor system.

(i) Initially, *reference frames* are established. N denotes the Newtonian frame, characterized by three unit vectors $\hat{\mathbf{n}}_x$, $\hat{\mathbf{n}}_y$, and $\hat{\mathbf{n}}_z$. Additionally, B_i represents a frame attached to the i^{th} blade, similarly characterized by $\hat{\mathbf{b}}_{ix}$, $\hat{\mathbf{b}}_{iy}$, and $\hat{\mathbf{b}}_{iz}$. Notably, in this method only frame orientations are relevant, disregarding frame positions. The relations between the reference frames are defined using generalized coordinates, revealing a significant connection between frame projections and the directional cosine matrix,

$$
{}^{N}\mathbf{C}^{B_i} = \begin{bmatrix} \hat{\mathbf{n}}_x \cdot \hat{\mathbf{b}}_{ix} & \hat{\mathbf{n}}_x \cdot \hat{\mathbf{b}}_{iy} & \hat{\mathbf{n}}_x \cdot \hat{\mathbf{b}}_{iz} \\ \hat{\mathbf{n}}_y \cdot \hat{\mathbf{b}}_{ix} & \hat{\mathbf{n}}_y \cdot \hat{\mathbf{b}}_{iy} & \hat{\mathbf{n}}_y \cdot \hat{\mathbf{b}}_{iz} \\ \hat{\mathbf{n}}_z \cdot \hat{\mathbf{b}}_{ix} & \hat{\mathbf{n}}_z \cdot \hat{\mathbf{b}}_{iy} & \hat{\mathbf{n}}_z \cdot \hat{\mathbf{b}}_{iz} \end{bmatrix} = \begin{bmatrix} \cos(q_4 + \Psi_i) & \sin(q_4 + \Psi_i) & 0 \\ -\sin(q_4 + \Psi_i) & \cos(q_4 + \Psi_i) & 0 \\ 0 & 0 & 1 \end{bmatrix}, \quad (i = 1, 2, 3) \tag{1}
$$

where ${}^{N}\mathbf{C}^{B_i}$ is the directional cosine matrix for frame B_i with respect to frame N, and $\Psi_1 = 0$, $\Psi_2 = 2\pi/3$ and $\Psi_3 = 4\pi/3$ are the initial azimuth angles of the three blades.

(ii) From the definition of reference frame orientations, *angular velocities and accelerations* are derived. Géradin et al. [16] proves that time-derivatives in the Newtonian frame, denoted as $\frac{{}^{N}d}{dt}$, to an arbitrary unit vector $\hat{\mathbf{b}}_{ik}$ can be expressed as,

$$
\frac{{}^{N}d}{dt}\hat{\mathbf{b}}_{ik} = \frac{{}^{N}d}{dt}{}^{B_i}\mathbf{C}^{N\,N}\mathbf{C}^{B_i}\hat{\mathbf{b}}_{ik}, \quad (i = 1, 2, 3)\ (k = x, y, z) \tag{2}
$$

which, due to the skew symmetric nature of $\frac{{}^{N}d}{dt}{}^{B_i}\mathbf{C}^{N\,N}\mathbf{C}^{B_i}$, is the matrix analog to the vector relationship,

$$
\frac{{}^{N}d}{dt}\hat{\mathbf{b}}_{ik} = {}^{N}\boldsymbol{\omega}^{B_i} \times \hat{\mathbf{b}}_{ik}, \quad (i = 1, 2, 3)\ (k = x, y, z) \tag{3}
$$

where $\times$ denotes the cross product, and ${}^{N}\boldsymbol{\omega}^{B_i}$ is the angular velocity of frame B_i with respect to frame N. The model-specific angular velocities ${}^{N}\boldsymbol{\omega}^{B_i}$ and accelerations ${}^{N}\boldsymbol{\alpha}^{B_i}$ read respectively,

$$
{}^{N}\boldsymbol{\omega}^{B_i} = \dot{q}_4\hat{\mathbf{n}}_z, \qquad {}^{N}\boldsymbol{\alpha}^{B_i} = \frac{{}^{N}d}{dt}{}^{N}\boldsymbol{\omega}^{B_i} = \ddot{q}_4\hat{\mathbf{n}}_z, \quad (i = 1, 2, 3) \tag{4}
$$

where $\dot{q}_4$ and $\ddot{q}_4$ are respectively the first and second time-derivative to the generalized coordinate q_4.

(iii) *Position vectors* from the origin O to each point in the model are oriented with unit vectors of the reference frames and scaled with generalized coordinates. In the context of this model, for point P_i on the tip of each blade, a specific position vector $\mathbf{p}^{OP_i}$ is defined,

$$
\mathbf{p}^{OP_i} = l_b\hat{\mathbf{b}}_{ix} + q_i\hat{\mathbf{b}}_{iy}, \quad (i = 1, 2, 3) \tag{5}
$$

(iv) Translational *velocities and accelerations* are derived for each point by the time-derivative in the N frame to the position vectors in (5). By making use of (3) the generic one-point theorem from [17] appears. Accordingly, the specific velocity ${}^{N}\mathbf{v}^{P_i}$ and acceleration ${}^{N}\mathbf{a}^{P_i}$ of each blade read,

$$
\begin{aligned}
{}^{N}\mathbf{v}^{P_i} = \frac{{}^{N}d}{dt}\mathbf{p}^{OP_i} &= {}^{N}\mathbf{v}^{O} + {}^{N}\boldsymbol{\omega}^{B_i} \times \mathbf{p}^{OP_i} + {}^{B_i}\mathbf{v}^{P_i} \\
&= \dot{q}_4(l_b\hat{\mathbf{b}}_{iy} - q_i\hat{\mathbf{b}}_{ix}) + \dot{q}_i\hat{\mathbf{b}}_{iy}, \qquad (i = 1, 2, 3)
\end{aligned} \tag{6}
$$

$$
\begin{aligned}
{}^{N}\mathbf{a}^{P_i} = \frac{{}^{N}d}{dt}{}^{N}\mathbf{v}^{P_i} &= {}^{N}\mathbf{a}^{O} + {}^{N}\boldsymbol{\alpha}^{B_i} \times \mathbf{p}^{OP_i} + {}^{N}\boldsymbol{\omega}^{B_i} \times ({}^{N}\boldsymbol{\omega}^{B_i} \times \mathbf{p}^{OP_i}) \\
&\quad + 2{}^{N}\boldsymbol{\omega}^{B_i} \times {}^{N}\mathbf{v}^{P_i} + {}^{B_i}\mathbf{a}^{P_i} \\
&= \ddot{q}_4(l_b\hat{\mathbf{b}}_{iy} - q_i\hat{\mathbf{b}}_{ix}) + \dot{q}_4^2(-l_b\hat{\mathbf{b}}_{ix} - q_i\hat{\mathbf{b}}_{iy}) - 2\dot{q}_4\dot{q}_i\hat{\mathbf{b}}_{ix} + \ddot{q}_i\hat{\mathbf{b}}_{ix}, \quad (i = 1, 2, 3)
\end{aligned} \tag{7}
$$

(v) *Generalized speeds* are chosen as linear combinations of generalized coordinate derivatives, in what Kane specifies as the kinematical differential equations. For this specific model, generalized speeds are chosen as,

$$\begin{bmatrix} u_1 \\ u_2 \\ u_3 \\ u_4 \end{bmatrix} = \begin{bmatrix} {}^{B_1}\mathbf{v}^{P_1} \cdot \hat{\mathbf{b}}_{1y} \\ {}^{B_2}\mathbf{v}^{P_2} \cdot \hat{\mathbf{b}}_{2y} \\ {}^{B_3}\mathbf{v}^{P_3} \cdot \hat{\mathbf{b}}_{3y} \\ {}^{N}\boldsymbol{\omega}^{B_1} \cdot \hat{\mathbf{b}}_{1z} \end{bmatrix} = \begin{bmatrix} \dot{q}_1 \\ \dot{q}_2 \\ \dot{q}_3 \\ \dot{q}_4 \end{bmatrix} \tag{8}$$

In this specific model, as opposed to 3D models, the generalized speeds u_i directly coincide with the generalized coordinate derivatives $\dot{q}_i$, which are replaced in the kinematic expressions of (4), (6) and (7).

(vi) *Active forces and torques* acting on the points are defined based on the unit vectors from the reference frames. Here the internal forces r_i from the stiffness and damping of the blades are revealed by splitting the blade model in Figure 2 into separate free body diagrams in Figure 3.

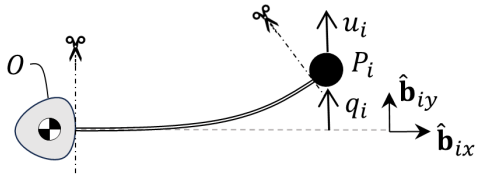

Figure 2: Blade model cut in free body diagrams.

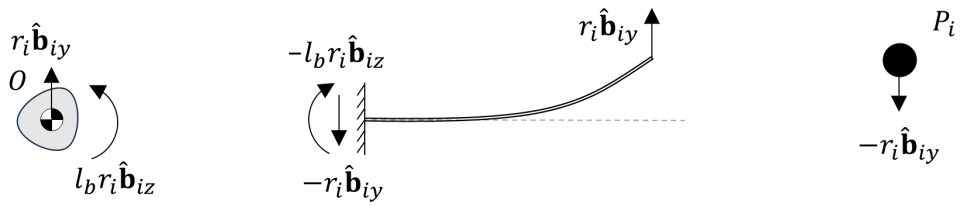

(a) (b) (c)

Figure 3: Free body diagram for a) hub in frame B_1 with center of mass in origin O, b) cantilever beam with tip displacement q_i and velocity u_i, and c) point P_i on blade tip.

In addition to restoring internal forces from the free body diagram, the active forces $\mathbf{f}^{P_i}$ and torque $\mathbf{t}^{B_1}$ are gathered from gearbox damping, gravity, and wind loads. Here, it is important to note that there are three points P_i, yet only one body B_1 is present. Accordingly,

$$\mathbf{f}^{P_i} = -r_i\hat{\mathbf{b}}_{iy} + m_b G(t)\hat{\mathbf{n}}_x + F_w(t)\hat{\mathbf{b}}_{iy}, \quad (i = 1, 2, 3) \tag{9}$$

$$\mathbf{t}^{B_1} = -d_g u_4\hat{\mathbf{b}}_{1z} + \sum_{i=1}^{3} r_i l_b\hat{\mathbf{b}}_{iz} \tag{10}$$

The restoring forces combine the impacts of blade stiffness and damping,

$$r_i = r_i^s + \zeta_b m_b u_i, \quad (i = 1, 2, 3) \tag{11}$$

where r_i^s denotes the static restoring forces arising from the bending stiffness of the blades. The inclusion of these static restoring forces as additional unknowns is pivotal in the transition from a pure numerical model to a hybrid model. Additionally, to prevent the simulation from showing the typical oscillation pattern of a step-response, the gravitational force $G(t)$ and wind loads $F_w(t)$ are ramped to their nominal value using exponential time-modulating functions,

$$G(t) = (1 - e^{-t/t_0})g, \quad F_w(t) = (1 - e^{-t/t_0})f_w \tag{12}$$

(vii) *Inertia forces* are defined for the lumped masses on the blade tips following the Newton formulation, and an *inertia torque* is defined for the body of the geartrain following the Euler formulation. Notably, both accelerations from (7) and angular accelerations from (4) are defined in the Newtonian frame N. Accordingly,

$$\mathbf{f}^{*P_i} = -m_b {}^N\mathbf{a}^{P_i}, \quad (i = 1, 2, 3) \tag{13}$$

$$\mathbf{t}^{*B_1} = -\mathbf{I}^{B_1} \cdot {}^N\boldsymbol{\alpha}^{B_1} - {}^N\boldsymbol{\omega}^{B_1} \times \left(\mathbf{I}^{B_1} \cdot {}^N\boldsymbol{\omega}^{B_1}\right), \quad \mathbf{I}^{B_1} = I_g \hat{\mathbf{b}}_{1z} \otimes \hat{\mathbf{b}}_{1z} \tag{14}$$

where $\mathbf{I}^{B_1}$ is the inertia dyadic of the body attached to frame B_1 around the origin O as seen from the frame itself.

(viii) *Partial velocities and angular velocities* are derived based on (4) and (6),

$${}^N\mathbf{v}_j^{P_i} = \frac{\partial^N \mathbf{v}^{P_i}}{\partial u_j}, {}^N\boldsymbol{\omega}_j^{B_1} = \frac{\partial^N \boldsymbol{\omega}^{B_1}}{\partial u_j}, \quad (j = 1, 2, 3, 4)(i = 1, 2, 3) \tag{15}$$

(ix) The *equation of motion* is next formulated based on the Kane method, projecting the active and inertia forces and torques from (9), (10), (13) and (14), onto the partial velocities from (15).

$$\sum_{i=1}^{3} {}^N\mathbf{v}_j^{P_i} \cdot (\mathbf{f}^{P_i} + \mathbf{f}^{*P_i}) + {}^N\boldsymbol{\omega}_j^{B_1} \cdot (\mathbf{t}^{B_1} + \mathbf{t}^{*B_1}) = 0, \quad (j = 1, 2, 3, 4) \tag{16}$$

(x) Finally, the EoMs from (16) are recasted in *state-space form* by combining them with the kinematical equations of (8). Accordingly,

$$\mathbf{f}(t, \dot{\mathbf{x}}, \mathbf{x}, r_1^s, r_2^s, r_3^s) = \begin{bmatrix} \dot{q}_1 - u_1 \\ \vdots \\ \dot{q}_4 - u_4 \\ \sum_{i=1}^{3} {}^N\mathbf{v}_1^{P_i} \cdot (\mathbf{f}^{P_i} + \mathbf{f}^{*P_i}) + {}^N\boldsymbol{\omega}_1^{B_1} \cdot (\mathbf{t}^{B_1} + \mathbf{t}^{*B_1}) \\ \vdots \\ \sum_{i=1}^{3} {}^N\mathbf{v}_4^{P_i} \cdot (\mathbf{f}^{P_i} + \mathbf{f}^{*P_i}) + {}^N\boldsymbol{\omega}_4^{B_1} \cdot (\mathbf{t}^{B_1} + \mathbf{t}^{*B_1}) \end{bmatrix} = \mathbf{0} \tag{17}$$

By constructing a generalized parameter vector with generalized coordinates and speeds, (16) is reconstructed to the generic form of first-order ordinary differential equations,

$$\mathbf{x} = \begin{bmatrix} q_1 \\ \vdots \\ q_4 \\ u_1 \\ \vdots \\ u_4 \end{bmatrix}, \quad \mathbf{M}(\mathbf{x})\dot{\mathbf{x}} + \mathbf{g}(t, \mathbf{x}, r_1^s, r_2^s, r_3^s) = \mathbf{0} \tag{18}$$

where $\mathbf{M}(\mathbf{x})$ is the mass matrix with a dependency on the generalized parameter vector $\mathbf{x}$,

$$\begin{aligned} \mathbf{M}(\mathbf{x}) &= \frac{\partial \mathbf{f}(t, \dot{\mathbf{x}}, \mathbf{x}, r_1^s, r_2^s, r_3^s)}{\partial \dot{\mathbf{x}}} \\ &= \begin{bmatrix} [\mathbf{I}]_{4\times4} & [\mathbf{0}]_{4\times4} \\ [\mathbf{0}]_{4\times4} & \begin{bmatrix} -m_b & 0 & 0 & -l_b m_b \\ 0 & -m_b & 0 & -l_b m_b \\ 0 & 0 & -m_b & -l_b m_b \\ -l_b m_b & -l_b m_b & -l_b m_b & -I_g - \sum_{i=1}^{3} m_b (l_b^2 + q_i^2) \end{bmatrix} \end{bmatrix} \end{aligned} \tag{19}$$

and $\mathbf{g}(t, \mathbf{x}, r_1^s, r_2^s, r_3^s)$ represents the vector of Coriolis, centrifugal and generalized active forces dependent on time t, generalized parameter vector $\mathbf{x}$, and crucially the static restoring forces r_1^s, r_2^s and r_3^s. Accordingly,

$$\begin{aligned} \mathbf{g}(t, \mathbf{x}, r_1^s, r_2^s, r_3^s) &= \mathbf{f}(t, \dot{\mathbf{x}}, \mathbf{x}, r_1^s, r_2^s, r_3^s) - \mathbf{M}(\mathbf{x})\dot{\mathbf{x}} \\ &= \begin{bmatrix} -u_1 \\ \vdots \\ -u_4 \\ (1 - e^{-t/t_0})(f_w - g m_b \sin(q_4 + \Psi_1)) - r_1^s - m_b \zeta_b u_1 + m_b q_1 u_4^2 \\ (1 - e^{-t/t_0})(f_w - g m_b \sin(q_4 + \Psi_2)) - r_2^s - m_b \zeta_b u_2 + m_b q_2 u_4^2 \\ (1 - e^{-t/t_0})(f_w - g m_b \sin(q_4 + \Psi_3)) - r_3^s - m_b \zeta_b u_3 + m_b q_3 u_4^2 \\ \sum_{i=1}^{3} \left((1 - e^{-t/t_0})(f_w l_b - g m_b q_i \cos(q_4 + \Psi_i)) + 2 m_b q_i u_i u_4 \right) - d_g u_4 \end{bmatrix} \end{aligned} \tag{20}$$

Lastly, the state-space formulation for the hybrid model is attained from solving for $\dot{\mathbf{x}}$ in (18),

$$\dot{\mathbf{x}} = \underbrace{-\mathbf{M}(\mathbf{x})^{-1} \mathbf{g}(t, \mathbf{x}, r_1^s, r_2^s, r_3^s)}_{\mathbf{f}^{rhs}(t, \mathbf{x}, r_1^s, r_2^s, r_3^s)} \tag{21}$$

where the right-hand-side function of the formulation is defined as $\mathbf{f}^{rhs}(t, \mathbf{x}, r_1^s, r_2^s, r_3^s)$.

The hybrid model has been derived in SymPy, which is a Python module for symbolic calculus. It provides a specific library for analytical mechanics based on the Kane method. The lecture notes on MBD by Prof. Moore [17] and the SymPy module [18] are extremely helpful to get quickly proficient with using the Python module.

3. Implementation of the hybrid model

A physical experiment was implemented based on the developed hybrid model, using a newly installed setup for HT at Dynamisk LAB of Aarhus University. In the hybrid test, one of the blades is represented by a PS, while the rest of the model is simulated within a NS. Specifically,

the static restoring force r_1^s is physically measured from a $500 \times 100 \times 5$ mm cantilever steel beam. The tip of the cantilever beam receives a displacement q_1 from the NS through an electromechanical actuator. Subsequently, a force transducer, positioned between the actuator and the PS, measures the restoring force. The actuator is characterized by 300 mm stroke and 10 kN force capacity, coinciding with the force transducer admissible load. Figure 4 provides an overview of the experimental setup.

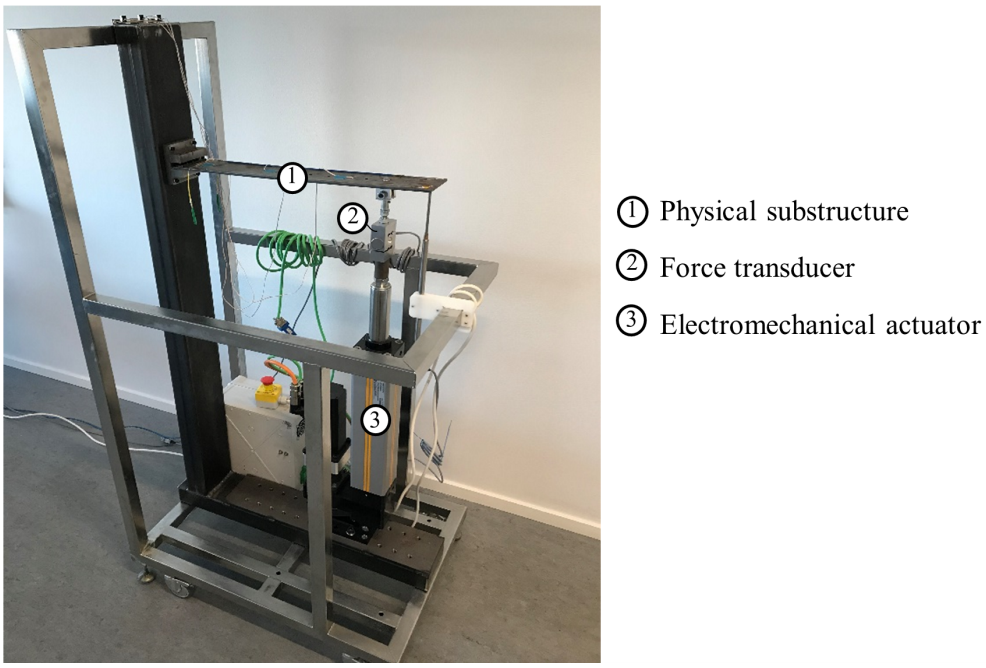

Figure 4: Single-degree-of-freedom testbench for hybrid testing at Dynamisk LAB of Aarhus University. The physical substructure of the rotor blade is represented by a cantilever beam.

The experimental setup was operated from a Beckhoff RT-industrial PC, using the EtherCAT protocol for communication with the actuator controller and force transducer. This facilitated a real-time processing-on-the-fly approach, incorporating a Python environment for sending actuator positions through an API control system and retrieving associated restoring force data. In Figure 5 the real-time system is visualized.

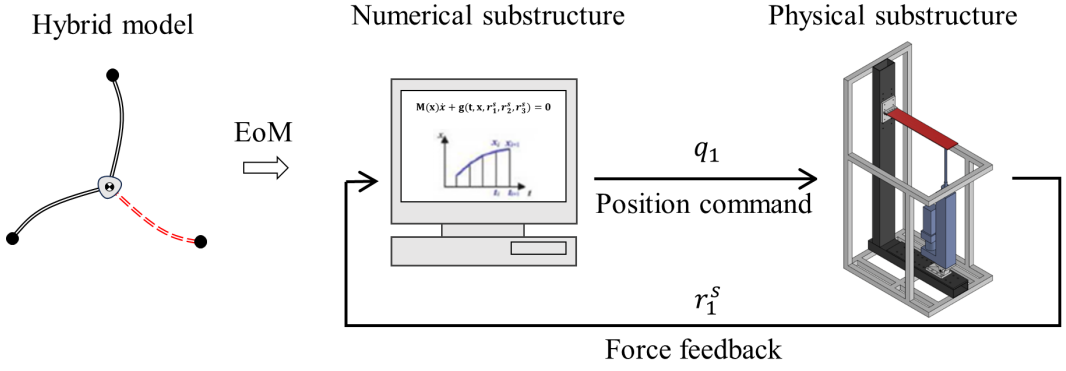

Figure 5: Schematic overview of a real-time system for hybrid testing.

The equation of motion from the hybrid model was solved using a 2nd order Runge-Kutta time integration scheme with a fixed time step of $h = 10\ ms$. The procedure for solving the equation of motion is provided below in the form of a pseudocode.

Algorithm 1 Runge-Kutta scheme for pseudo-dynamic Hybrid Testing.

Initialize $n \leftarrow 1$
Initialize $\mathbf{x}_n \leftarrow \mathbf{x}_0$
while $n < N_{steps}$ **do**
  Initialize $i \leftarrow 1$
  while $i < s$ **do**
    Compute state $\mathbf{x}_n^i = \mathbf{x}_n + h \sum_{j=1}^{i-1} a_{i,j} \mathbf{k}_j$
    Extract blade displacements $q_1 = \mathbf{x}_n^i(1)$, $q_2 = \mathbf{x}_n^i(2)$ and $q_3 = \mathbf{x}_n^i(3)$
    Send actuator position command $q_1 + p_0$
    Retrieve restoring force feedback r_1^s from PS
    Compute restoring force $r_2^s = k_b q_2$ from NS
    Compute restoring force $r_3^s = k_b q_3$ from NS
    Compute $\mathbf{k}_i = \mathbf{f}^{rhs}(t_n + c_i h, \mathbf{x}_n + h \sum_{j=1}^{i-1} a_{i,j} \mathbf{k}_j, r_1^s, r_2^s, r_3^s)$
    Update $i \leftarrow i + 1$
  end while
  Update $\mathbf{x}_{n+1} \leftarrow \mathbf{x}_n + h \sum_{i=1}^{s} b_i \mathbf{k}_i$
  Update $t_{n+1} \leftarrow t_n + h$
  Update $n \leftarrow n + 1$
end while

where a_{ij}, b_i and c_i are coefficients of the Runge-Kutta method extracted from a Butcher Table (e.g., from [19]), p_0 is the initial position of the actuator, which corresponds to a zero restoring force, and N_{steps} is the number of steps. The main advantage of using an explicit Runge-Kutta scheme is that the Jacobian of $\mathbf{f}^{rhs}(t, \mathbf{x}, r_1^s, r_2^s, r_3^s)$ w.r.t. the hybrid model state vector $\mathbf{x}$ is not computed and the solution algorithm does not require iterations to converge. This is a particularly important feature for MBD hybrid models given that also the mass matrix is nonlinear and an operator-splitting-like approach [20] might not be sufficiently accurate.

4. Results and discussion

To verify the hybrid model implementation, a dummy HT was conducted, where the PS was temporally substituted by a NS. When the results perfectly matched with a reference response history analysis, the static restoring force r_1^s was linked to the force transducer measurement. A HT was thereby successfully conducted by implementing the hybrid model through the proposed algorithm. The dynamic behavior was simulated for the WT rotor within a 10 s duration using a time step of 0.001 s. The hybrid test lasted 6 hours and 16 minutes, that is, about 2260 slower than real-time (pseudo-dynamic regime). Results from the generalized coordinates, q_1, q_2 and q_3 dictating the displacement of the blades are presented in Figure 6a, and the generalized speed u_4 representing the angular velocity of the hub is presented in Figure 6b. In Figure 7 the results from a pure numerical simulation of the same simplified WT rotor system are presented.

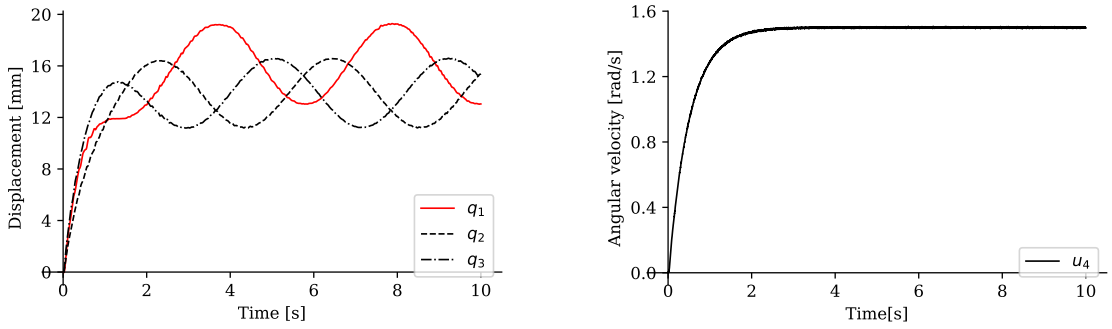

(a) (b)

Figure 6: Hybrid test results of a) generalized coordinates q_1, q_2 and q_3 representing the blade-tip displacements, where the red line indicates the displacement from the PS, and b) generalized speed u_4 representing the angular velocity of the hub.

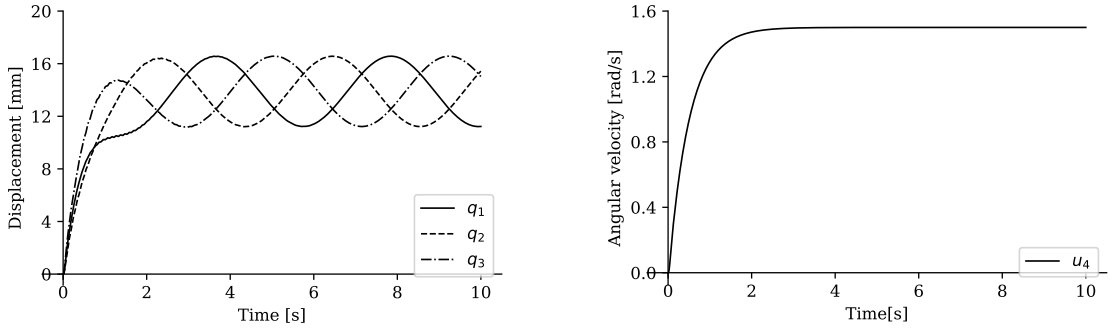

(a) (b)

Figure 7: Numerical simulation results of a) generalized coordinates q_1, q_2 and q_3 representing the blade-tip displacements and b) generalized speed u_4 representing the angular velocity of the hub.

The displacement history of the three blades, shown in Figure 6a, differs from the displacement of the same blades in the purely numerical simulation shown in Figure 7a. The motion history q_1 of the PS blade exhibits a larger amplitude and average displacement compared to the numerical simulation. This suggests a lower stiffness for the blade in the PS than those in the NS. As seen by a small oscillation in the HT in Figure 6b, when compared to the numerical simulation in 7b, the derivation in blade displacement has a small influence on the angular velocity. As one can note, after the initial transient, the response of the blades is periodic, which indicates that the numerical integration scheme produces stable results.

5. Conclusion

This study provided a practical demonstration of the Kane method's efficiency in implementing hybrid testing for wind turbine mechanical components. The introduction of static restoring forces as additional variables in the multi-body-dynamic hybrid model formulation proved to be very efficient. Such variables can be efficiently linked to physical measurements while running a hybrid test by substituting with analytical expression in the test verification phase. The implementation on a 1-degree-of-freedom test bench using an explicit Runge-Kutta scheme demonstrated that a stable experiment can be performed in the pseudo-dynamic regime.

References

[1] M. Hansen, Aerodynamics of Wind Turbines: second edition, 2nd Edition, Earthscan, 2008.

[2] M. Hakuno, M. Shidawara, T. Hara, Dynamic destructive test of a cantilever beam, controlled by an analog computer, 1969.

[3] K. Takanashi, K. Udagawa, M. Seki, T. Okada, H. Tanaka, Non-linear earthquake response analysis of structures by a computer-actuator on-line system, Transaction of the Architectural Institute of Japan 229 (1975) 77–83.

[4] P. Pan, T. Wang, M. Nakashima, Development of Online Hybrid Testing: Theory and Applications to Structural Engineering, 2015.

[5] C. Gomes, C. Thule, D. Broman, P. G. Larsen, H. Vangheluwe, Co-simulation: A survey 51 (3) 1–33. doi:10.1145/3179993.

[6] D. Bosse, R. Schelenz, D. Radner, G. Jacobs, Analysis and application of hardware in the loop wind loads for full scale nacelle ground testing, 2013.

[7] J. Cheon, J. Kim, J. Lee, K. Lee, Y. Choi, Development of hardware-in-the-loop-simulation testbed for pitch control system performance test, Energies 12 (10) (2019). doi:10.3390/en12102031.

[8] T. Sauder, V. Chabaud, M. Thys, E. Bachynski-Polić, L. Sæther, Real-time hybrid model testing of a braceless semi-submersible wind turbine: Part i — the hybrid approach, 2016, p. V006T09A039. doi:10.1115/OMAE2016-54435.

[9] M. Belloli, I. Bayati, A. Facchinetti, A. Fontanella, H. Giberti, F. La Mura, F. Taruffi, A. Zasso, A hybrid methodology for wind tunnel testing of floating offshore wind turbines, Ocean Engineering 210 (2020) 107592. doi:https://doi.org/10.1016/j.oceaneng.2020.107592.

[10] T. Kane, C. Wang, On the derivation of equations of motion, Journal of the Society of Industrial and Applied Mechanics 13 (2) (1965) 487–492.

[11] T. Kane, D. Levinson, Formulation of equations of motion for complex spacecraft, Journal of Guidance, Control, and Dynamics 3 (2) (1980) 99–112.

[12] J. Jonkman, M. Sprague, colleagues of NREL, OpenFAST — wind research — NREL, accessed: 2024-01-02 (2024).
URL `https://www.nrel.gov/wind/nwtc/openfast.html`

[13] DTU Wind Energy, HAWC - Horizontal Axis Wind turbine simulation Code 2nd generation, accessed: 2024-01-11 (2024).
URL `https://www.hawc2.dk/about-hawc2`

[14] A. Banerjee, Flexible Multibody Dynamics: Efficient Formulations with Applications, 2nd Edition, CRC Press, 2022. doi:10.1201/9781003231523.

[15] C. Roithmayr, D. H. Hodges, Dynamics: Theory and Application of Kane's Method, Cambridge University Press, 2016.

[16] M. Géradin, A. Cardona, Flexible Multibody Dynamics: A Finite Element Approach, Vol. 4, 2001.

[17] J. K. Moore, Learn multibody dynamics (2022).
URL `https://moorepants.github.io/learn-multibody-dynamics/`

[18] SymPy Development Team, Sympy documentation, accessed on January 16, 2024 (2023).
URL `https://docs.sympy.org/latest/index.html`

[19] J. C. Butcher, A stability property of implicit runge-kutta methods 15 (4) 358–361. doi:10.1007/BF01931672.

[20] G. Abbiati, I. Lanese, E. Cazzador, O. S. Bursi, A. Pavese, A computational framework for fast-time hybrid simulation based on partitioned time integration and state-space modeling, Structural Control and Health Monitoring 26 (10) (2019).